Applied Catalysis B: Environmental 181 (2016) 34–46

Contents lists available at ScienceDirect

Applied Catalysis B: Environmental

journal homepage: www.elsevier.com/locate/apcatb

Catalyst development for steam reforming of methane and model biogas at low temperature

Sofia D. Angeli[a], Luca Turchetti[b], Giulia Monteleone[b], Angeliki A. Lemonidou[a,*]

[a] Department of Chemical Engineering, Aristotle University of Thessaloniki, University Campus, GR-54124 Thessaloniki, Greece
[b] ENEA, Italian National Agency for New Technologies, Energy and Sustainable Economic Development, Technical Unit for Renewable Energy Sources (UTRINN), via Anguillarese 301, 00123 Rome, Italy

ARTICLE INFO

Article history:
Received 9 March 2015
Received in revised form 17 July 2015
Accepted 24 July 2015
Available online 26 July 2015

Keywords:
Methane steam reforming
Ni catalyst
Rh catalyst
Ceria-zirconia
La dopant

ABSTRACT

Low temperature steam reforming (400–550 °C) for the production of hydrogen offers significant advantages compared to the conventional process. The milder operating conditions lead to lower operation costs and cost of construction materials. Additionally, no CO shift reactor is required due to favorable temperature for the WGS reaction. In this work, we report the catalytic performance of Ni and Rh catalysts supported on La_2O_3–ZrO_2 and La_2O_3–CeO_2–ZrO_2 for their application in a multifuel membrane reformer operating at low temperature. The performance of the catalysts is assessed in different operating conditions in methane steam reforming (GHSV, temperature, H_2O/CH_4 ratio) as well as in reforming of model biogas. Stability tests were conducted up to 90 h on stream (1 bar and 7 bar) and the tendency toward carbon formation was investigated. All catalysts were active in the reforming reactions at 400–550 °C and the catalysts supported on La_2O_3–CeO_2–ZrO_2 showed superiority in activity and stability probably due to the presence of ceria in the support which contributes to the reforming rate and the resistance to carbonaceous deposits. Ni(10)CeZrLa exhibited remarkably stable performance with minimum amount of carbon formed after 90 h (ca. 0.05 wt%). TPO and TPH analysis of the carbonaceous deposits showed that the dominating type of carbon is highly reactive and can be easily removed by oxidation or hydrogenation at 500 °C. This fact makes the catalyst even more promising for the proposed low temperature process, since the catalyst can be hydrogenated by using part of the H_2 production stream without further heating of the reactor.

1. Introduction

Hydrogen is a very important raw material in chemical industries and refineries but also an energy carrier. Steam reforming plays a key role in the production of hydrogen using as primary feedstock natural gas or its renewable counterpart; biogas [1,2].

In the conventional process, natural gas reacts with steam at temperatures over 800 °C in the presence of a nickel catalyst [3–5]. The main reaction product is syngas, a mixture of hydrogen and carbon monoxide, which is used as a raw material for the production of other organic chemicals. When hydrogen is the desired product, syngas from the reformer is fed to a water-gas shift reactor where carbon monoxide reacts with steam over a catalyst to produce more hydrogen and carbon dioxide. Finally, the produced gas mixture is sent to a pressure swing absorption unit (PSA) to achieve pure hydrogen. The requirement of elevated temperature due to the endothermic character of the reforming reaction result in low energy efficiency, high operation cost and emissions of greenhouse gases (GHG).

A new process has been recently proposed aiming at the intensification of methane steam reforming [6]. This process is focused on the production of pure hydrogen via steam reforming at the temperature range of 400–550 °C. The milder operating conditions offer significant advantages such as lower operation costs and cost of materials. Furthermore, the temperature conditions applied, favor the water gas shift (WGS) reaction, thus separate CO shift reactor is not required. On the other hand, thermodynamic limitations result in low conversions of methane and consequently in low H_2 yield. In order to shift the obtained conversion, the system is equipped with a hydrogen-selective membrane. As a result, hydrogen is separated with high purity from the product stream in one step, and at the same time the equilibrium of the reforming reaction is shifted

* Corresponding author. Fax: +30 2310996184.
E-mail addresses: saggeli@auth.gr (S.D. Angeli), luca.turchetti@enea.it (L. Turchetti), giulia.monteleone@enea.it (G. Monteleone), alemonidou@cheng.auth.gr (A.A. Lemonidou).

http://dx.doi.org/10.1016/j.apcatb.2015.07.039
0926-3373/

to the product side [7,8]. Experimental and modeling studies in the proposed system have shown that obtained conversion can be shifted to the value of 80–90% [9,10]. However, the use of a Pd-based membrane increases the total cost of the process.

Further reduction of GHG emissions is achieved by using concentrating solar power (CSP) plants as external carbon-free heat supplier. The utilization of molten salts up to 550 °C with a heat storage system can ensure constant-rate solar heat supply even for an energy demanding industrial chemical process like the steam reforming of methane [11]. Moreover, in order to use hydrogen as an energy carrier, a transition period comprising both renewable and fossil sources will exist. Accordingly, the compact small-scale process proposed offers flexibility to use as primary fuel natural gas, biogas or bioethanol according to local availability.

One of the key factors contributing to the success of such an integrated system for hydrogen production is the use of reforming catalysts that show high activity at such low temperatures and suppress coke formation reactions as well. Ni-based catalysts are the most common catalysts for the reforming process due to their high activity and low cost [2,12]. Noble metals are generally more active than Ni in the reforming reaction but their high cost has prevented their establishment in the industrial application [13]. However, it is well known that both the metal type and the support can contribute to the characteristic properties of an ideal reforming catalyst [2]. Some state-of-the-art supports such as alumina, are not so efficient in the dissociation of water in H and OH groups, so they can only be applied in high temperature reforming [14].

In steam reforming of methane, zirconia has been reported as promising support due to the accumulation of water on the surface and the formation of hydroxyl groups at 500 °C [15]. Reducible supports such as CeO_2 and CeO_2–ZrO_2 mixed oxides are also good candidates for low temperature MSR due to the active role in the redox mechanism through the mobility of surface oxygen species [16–23]. The oxygen storage capacity of CeO_2–ZrO_2 can be improved by the addition of La [24] thus, enhancing the resistance toward carbon formation [25,26] and the thermal stability of the catalyst [27].

Biogas reforming is an attractive feedstock for the utilization of biogas and the production of hydrogen, especially due to its renewable nature. The most commonly studied process for the reforming of biogas is dry reforming, in which the main components (CH_4 and CO_2) contribute to the production of syngas [28,29]. Steam reforming of biogas has also been investigated [30,31], but there are only few experimental data in the low temperature range [32].

In this work, we report the catalytic performance of Ni and Rh catalysts supported on La_2O_3–ZrO_2 and La_2O_3–CeO_2–ZrO_2 in view of their application in a multifuel membrane reformer operating at low temperature. Both the activity and stability of the catalysts are assessed at different operating conditions, as well as their tendency toward the formation of carbonaceous deposits.

2. Experimental

2.1. Catalyst preparation

The catalysts investigated in this work were prepared via the wet impregnation method. As precursors of the active metals, $Ni(NO_3)_2{\cdot}6H_2O$ (Merck) and $RhCl_3{\cdot}3H_2O$ (Pressure Chemical) were used to obtain metal loading of 10 wt% in the case of Ni-based catalysts and 1 wt% in the case of Rh-based catalysts. Lanthanum doped cerium–zirconium oxide (78 wt% ZrO_2, 17 wt% CeO_2, 5 wt% La_2O_3, Mel Chemicals) and lanthanum doped zirconium hydroxide (oxide-based composition: 90 wt% ZrO_2, 10 wt% La_2O_3, Mel Chemicals) were used as catalyst supports, while the latter was precalcined under air flow at 800 °C for 4 h in order for the oxide to be formed. The supports were either sieved or pelletized and then crushed and sieved, in order to obtain a particle size of 250–355 μm. The aqueous solution of the metal precursor was mixed with the support particles and stirred for 1 h at 70 °C. The solvent was removed via evaporation under mild vacuum conditions followed by drying overnight at 120 °C. The catalytic materials supported on La_2O_3–CeO_2–ZrO_2 were calcined in air flow at 800 °C for 5 h while those supported on La_2O_3–ZrO_2 were calcined at lower temperature (600 °C) due to precalcination of the support. In the following text, the catalysts are referred to as M(*x*)CeZrLa for those supported on La_2O_3–CeO_2–ZrO_2 and to M(*x*)ZrLa for those supported on La_2O_3–ZrO_2, where M is the active metal and *x* the metal loading %wt.

2.2. Catalyst characterization

The surface area of the prepared materials was measured by N_2 adsorption at 77 K, using the multipoint BET analysis method with an Autosorb-1 Quantachrome flow apparatus. The samples were dehydrated in vacuum at 250 °C overnight, before surface area measurements. X-ray diffraction (XRD) patterns were obtained using a Siemens D500 diffractometer, with Cu Kα radiation, in order to identify the crystalline phases apparent. The crystallite size was calculated using XRD data by the Scherrer equation.

Temperature Programmed Reduction (TPR) experiments were performed in a gas flow system using a U-tube reactor connected online with a quadrupole mass analyzer (Omnistar). The catalyst sample (100 mg) was placed in the reactor and pretreated for 0.5 h at 250 °C followed by cooling at room temperature in He flow. The temperature was then raised from ambient to 800 °C at a rate of 10 °C/min in a 10% H_2/He flow (50 mL/min). The mass numbers (*m*/*z*) 2 and 18 were used for H_2 and H_2O monitoring, respectively.

The metal dispersion was measured through H_2 temperature-programed desorption (TPD-H_2). Using the same flow system as mentioned above, the catalysts (200 mg) were reduced in 20% H_2/He for 1 h at 550 °C to simulate the reduction treatment prior to the catalytic tests. After reduction, the sample was heated at 600 °C in He flow to desorb any H_2 that might have been spilled over the support and then was cooled to ambient temperature. The chemisorption step took place under a flow of 10% H_2/He for 1 h at 25 ± 2 °C. The temperature of adsorption was selected in order to minimize the effect of hydrogen spillover in La_2O_3–CeO_2–ZrO_2 support. The minimization of the latter effect has been thoroughly investigated in literature over noble metal catalysts supported on ceria-related materials and the main conclusions are that the adsorption temperature of −78 °C is required to suppress hydrogen spillover [33] and that when the reduction temperature is as high as 500 °C the spillover effect is significantly slowed down without suppression of the chemisorption on Rh due to SMSI [34]. It has also been shown for Rh/CeO_2 catalysts that after reduction at 500 °C, the metal remains chemically active and hydrogen adsorption would only take place on the metal both at adsorption temperature of −82 °C (191 K) and 25 °C (298 K) [35]. In this work, the reduction temperature is higher than 500 °C (550 °C), but it was selected so as to simulate the reduction process prior to each catalytic test. Especially for noble metal catalysts, the spillover effect is expected to be higher, but on the other hand, the use of $RhCl_3$ as precursor strongly inhibits this [35,36]. However, even though there are several publications reporting the measurement of Ni dispersion at adsorption temperature below 50 °C [19,37,38], the effect on hydrogen spillover has not been discussed. The TPD analysis was carried out in a heating rate of 10 °C/min until the temperature of 850 °C. In order to determine the amount of H_2 desorbed, the peak area was compared to that obtained when known amount of H_2 was pulsed. For the calculation of the moles of metal on the surface, the atomic ratio H:M of 1:1 was used. The specific surface area of metal

for each catalyst was based on the consideration that the area occupied by a surface metal atom is 6.51 Å^2 and 7.58 Å^2 for Ni and Rh respectively [39].

2.3. Catalytic evaluation

The flexibility of a compact reformer to be used for the production of hydrogen from different types of fuels is of high importance. In this work, natural gas (CH_4) and simulated biogas (molar ratio CH_4/CO_2 = 50/50) were selected as reforming feedstock for the evaluation of the proposed catalysts. Methane steam reforming experiments were conducted at Aristotle University of Thessaloniki (Thessaloniki, Greece) while the tests of biogas steam reforming were realized at the Italian National Agency for New Technologies, Energy and Sustainable Economic Development (Rome, Italy). The activity toward the conversion of each feed type was tested at the temperature range of 400–550 °C at atmospheric pressure and methane partial pressure of 0.25–0.5 (H_2O/CH_4 ratio of 1–3). Steam to carbon (H_2O/CH_4) of 3 was used in most of the tests, as it is commonly used in industrial reforming applications. The stability of the catalysts was assessed using biogas as reforming fuel, in order to obtain harsh conditions, since the presence of CO_2 may enhance the formation of coke [40,41].

Methane steam reforming experiments were performed at atmospheric pressure in a laboratory unit equipped with a mass flow-controlled system for gases admission (CH_4 for the reforming reaction and H_2 and He for the reduction of the catalyst), a fixed bed quartz reactor, and an online gas chromatograph. An UFLC pump (Shimadju) was used for the feeding of water to the reactor through a preheated line. The fixed bed reactor was heated electrically by a tubular furnace, with three independently controlled temperature zones. The temperature in the middle of the catalytic bed was measured with a coaxial thermocouple. The hot gases exiting the reactor were cooled for the unreacted steam to be condensed. The gas phase products were analyzed with an online gas chromatograph (Agilent Technologies 7890A) equipped with a TCD. To separate the products, two columns were used; PoraPlotQ for CO_2 and MS 5A for H_2, CO and CH_4.

Steam reforming of model biogas experiments were carried in a stainless steel fixed bed-tubular reactor with an inner diameter of 12 mm, where the catalyst is loaded on a stainless steel microporous plate. The gaseous reactants were fed from the top of the reactor, the flow rates of which were controlled by mass flow controllers for each component. Liquid H_2O is evaporated and mixed with the gaseous reactants (CH_4 and CO_2) within the hot box of the apparatus before entering the reactor, which is kept at 200 °C. The reaction temperature was measured with a coaxial thermocouple in the center of the catalytic bed and maintained through a ceramic heater. The pressure of reaction was controlled by a pressure regulator, installed at the outlet of the reactor. The reactor outlet stream was sent to a condenser to remove water and then analyzed through an online Advance Optima 2000 (ABB, Zurich, Switzerland) continuous industrial process analyzer, equipped with three different detectors: thermal conductivity, electrochemical cell and infrared, for monitoring the concentration of H_2, CH_4, CO, and CO_2 in the outlet dry gas.

Before the reaction, the catalysts were reduced in situ in a mixture of H_2 and He or N_2 at 550 °C for 1 h. The activity of the catalysts in methane and model biogas steam reforming was investigated at ambient pressure in the temperature range of 400–550 °C, H_2O/CH_4 molar ratio of 3 and GHSV of 30,000–70,000 h^{-1}. The stability of the catalysts was evaluated in model biogas steam reforming at the reference temperature of 500 °C, ambient pressure, H_2O/CH_4 of 3 and GHSV of 30,000 h^{-1}. The most promising catalysts in terms of activity and stability toward fuel reforming, were subsequently tested under more severe conditions (model biogas feed, P = 7 bar, H_2O/CH_4 = 3, GHSV = 30,000 h^{-1}) in order to investigate the resistance in the formation of carbonaceous deposits.

The performance of the catalysts is expressed in terms of methane conversion and is evaluated by comparison to that predicted by thermodynamic equilibrium. The equilibrium methane conversion was calculated through the minimization of the Gibb's free energy by employing Aspen Plus 11.1 software. The RGibbs reactor has been selected for the calculations, using the Peng–Robinson property method.

The conversion of methane was calculated from the composition of the effluent dry gas as follows:

$$X_{CH_4}, \% = \left(1 - \frac{[CH_4]_{out}}{\alpha \times ([CH_4]_{out} + [CO_2]_{out})}\right) \times 100$$

where α is the methane content in the fuel (i.e., 0.5 for model biogas and 1 for pure methane).

The surface rate of methane consumption is defined as the rate of consumed methane per surface area of active metal:

$$r_{CH_4} = \frac{X_{CH_4} \times F_{CH_4,in}}{SSA_{metal} \times m_{cat}}$$

where $F_{CH_4,in}$ is the molar flowrate of methane in the inlet of the reactor, X_{CH_4} the conversion of methane, SSA_{metal} the specific surface area of the active metal, and m_{cat} the mass of catalyst.

The deactivation of the catalysts in long-term stability test was calculated based on the conversion of methane at the beginning of the reaction (X_0) and at time t (X_t):

$$\text{Deactivation}, \% = \left(\frac{X_0 - X_t}{X_0}\right) \times 100$$

2.4. Characterization of used catalysts

Coke depositions on the used catalysts were qualitatively and quantitatively characterized via temperature programmed oxidation (TPO) and Temperature Programmed Hydrogenation (TPH) using the same experimental apparatus as in TPR tests described above. The used catalysts were pretreated at 250 °C for 0.5 h in He flow and allowed to cool. The samples were then heated in the rate of 10 °C/min to 850 °C in a flow of 50 mL/min of oxidation gas for the TPO or in a flow of hydrogenating gas for the TPH method. During the TPO test the mass numbers (m/z) 44 was used for monitoring the produced CO_2, while in the case of TPH, mass number (m/z) 15 was used for the monitoring of produced CH_4, instead of 16, due to no contribution of other gases. Quantification analysis of the carbonaceous species was realized by comparing the peak area of produced gas (CO_2 or CH_4) to that of known amount (250 μL) pulsed into the system.

The morphologies of the used catalysts after long-term stability test at steam reforming of simulated biogas at high pressure were observed in a JEOL 2011 transmission electron microscope (TEM), coupled with an Oxford Instruments INCAx-sight liquid nitrogen cooled EDS detector for detailed elemental analysis.

3. Results and discussion

3.1. Catalyst characterization

The characteristic properties of the prepared catalysts are shown in Table 1. The impregnation of the metals resulted in decrease in the specific surface area of the pure support. This is the result of pore blockage by the metal particles, especially in the case of Ni, due to the higher loading (10 wt%) with respect to that of Rh (1 wt%). In the case of CeZrLa support, the measurement of SSA was realized before any calcination procedure (as received). As

Table 1
Characteristic properties of the catalysts and the supports.

Sample	Active metal loading (%)	Specific surface area (m^2/g)	Dispersion (%)	Metal surface area (m^2_M/g_{cat})
Ni(10)ZrLa	Ni-10%	45.07	1.62	1.08
Rh(1)ZrLa	Rh-1%	51.76	29.09	1.29
ZrLa support (calcined at 800 °C, air, 5 h)	–	54.89	–	–
Ni(10)CeZrLa	Ni-10%	37.17	1.20	0.80
Rh(1)CeZrLa	Rh-1%	41.64	19.06	0.85
CeZrLa support	–	62.05	–	–

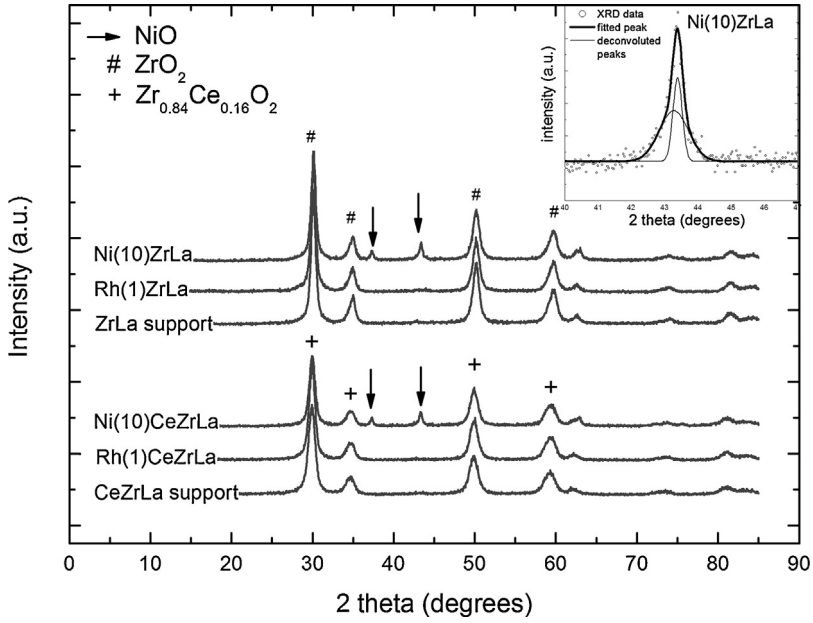

Fig. 1. X-ray diffraction patterns of the prepared catalysts and the supports. Inset graph: detail of the diffraction pattern of Ni(10)ZrLa in the diffraction angle (2θ) range 40–46° corresponding to NiO peak.

a result, not only the deposition of the metals, but also the calcination procedure applied to the CeZrLa-catalysts have contributed to the decrease in SSA.

Metal dispersion, as calculated based on H_2-TPD data, is higher for Rh based catalysts, possibly due to the much lower metal loading, especially for Rh(1)ZrLa.

The X-ray diffractograms of the catalysts and the supports are shown in Fig. 1. The characteristic peaks of $Zr_{0.84}Ce_{0.16}O_2$ and ZrO_2 appeared for the catalysts supported on the La_2O_3–CeO_2–ZrO_2 and La_2O_3–ZrO_2, respectively. No peaks for La_2O_3 were identified, probably due its amorphous state and the low loading. Diffractograms of the Ni-based catalysts exhibit the characteristic peaks of NiO in addition to that of the support. The crystallite size of NiO, as calculated by the Scherrer equation, in Ni(10)ZrLa was ca. 15 nm and in Ni(10)CeZrLa was ca. 18 nm. This observation is in agreement with the results of H_2-TPD; dispersion on the Ni based catalysts was very similar and the Ni crystallite size of Ni(10)ZrLa is expected to be slightly lower than that of Ni(10)CeZrLa. However, surface modification during the reduction process may affect the crystallite size of Ni. No Rh_2O_3 or any other form was detected by XRD in the Rh-based catalysts due to its low content.

In Fig. 2, the TPR profiles of the supports and the catalysts are presented. For the ZrLa support no reduction peak is observed, indicating that zirconia is not an easily reducible oxide [42,43]. Rh(1)ZrLa is characterized by a weak reduction peak at about 180 °C assigned to the reduction of RhO_x species, which is in good agreement with the literature [42]. The TPR profile of Ni(10)ZrLa reveals two peaks caused by the reduction of NiO characterized by different interactions with the support. As a result, the peak observed at 355 °C is ascribed to relatively "free" NiO, while the peak at 485 °C to

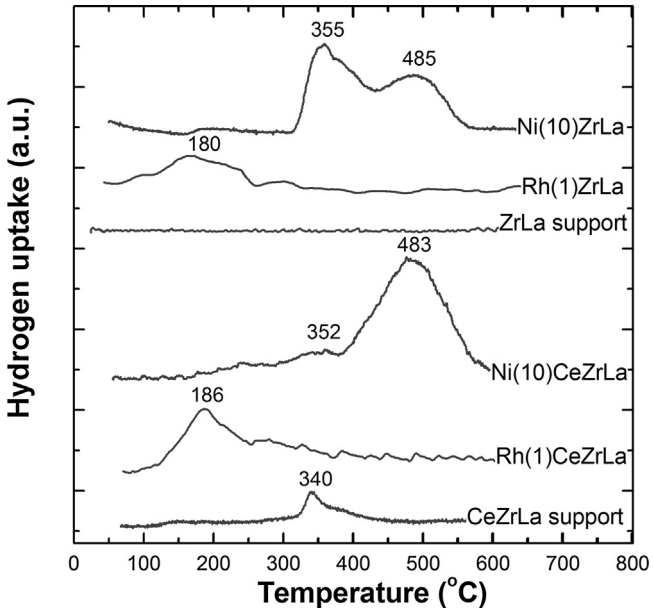

Fig. 2. Temperature Programmed Reduction profiles of the catalysts and the supports.

NiO species in intimate contact with the oxide support [44–46]. The differences in the interaction with the support imply the presence of NiO crystallites of different size. Under this consideration, the XRD data of Ni(10)ZrLa were further analyzed. The inset graph in Fig. 1 presents detail of the profile at diffraction angle (2θ) in range

Table 2
Hydrogen consumption during temperature programmed reduction.

Sample	Hydrogen consumption (mmol g_{cat}^{-1})		
	Ce[a]	Ni	Rh
Ni(10)ZrLa	–	1.696	–
Rh(1)ZrLa	–	–	0.127
ZrLa support	–	–	–
Ni(10)CeZrLa	0.271 (61)	1.704	–
Rh(1)CeZrLa	0.269 (55)	–	0.145
CeZrLa support	0.310 (63)	–	–

[a] Numbers in brackets refer to the molar percentage % of Ce^{4+} reduced to Ce^{3+} during TPR.

of 40–46°, where the main peak of NiO is apparent. The profile can be fitted by two peaks of the same maximum but of different width, corresponding to large- and small-sized crystallites [47] (35 nm and 10 nm, respectively), in agreement with the TPR results.

The TPR profiles of the CeZrLa support and the catalysts supported on it are also shown in Fig. 2. The TPR profile of the CeZrLa support is characterized by a single peak at 340 °C due to partial reduction of CeO_2 from Ce^{4+} to Ce^{3+} (Table 2). For the Rh-based catalyst, the main peak at 110–250 °C is the result of the reduction of Rh_2O_3 [46]. However, the quantification of hydrogen consumption during TPR showed that the amount of hydrogen consumed by the temperature of 250 °C is higher than that required for the complete reduction of Rh_2O_3 to metallic Rh (0.146 mmol H_2/g nominal consumption). Therefore, metal reduction and partial reduction of the support occur concurrently due to hydrogen spillover. The reduction degree of Ce^{4+} to Ce^{3+} by the temperature of 250 °C is quantified to 13%. The low intensity shoulder appeared in the TPR profile (up to 350 °C) is also ascribed to the reduction of the support realized at lower temperature than that of CeZrLa bare support due to the presence of the metal and hydrogen spillover effect [46,48]. By the temperature of 350 °C the total reduction degree of Ce^{4+} to Ce^{3+} reaches the value of 55% (Table 2). The TPR profile of Ni(10)CeZrLa reveals a low intensity peak at 352 °C and a high intensity peak centered at 483 °C. The position of the peaks is similar to that of Ni(10)ZrLa TPR profile, thus it could be ascribed to the reduction of NiO with different interaction with the support. On the other hand, quantification of the deconvoluted peaks showed that hydrogen consumption of the high-temperature peak corresponds to full reduction of NiO (1.704 mmol H_2/g nominal consumption). As a result, the low temperature peak is attributed to the partial reduction of the support [49], being also in agreement with the TPR profile of CeZrLa support. According to the quantification of TPR, the reducibility of the support is not affected by the impregnation of Ni but it is slightly decreased by the presence of Rh (Table 2). This is probably due to the synergistic effect of the presence of metal (positive) and the high-temperature calcination applied for the preparation of the catalysts (negative effect).

3.2. Methane steam reforming

The performance of the catalysts in low temperature steam reforming was first evaluated using methane as feed at atmospheric pressure and H_2O/CH_4 ratio of 3 at the temperature range of 400–550 °C and GHSV 30,000–70,000 h^{-1}.

In order to compare the catalysts, non-equilibrium conditions should be applied. As a result, tests at 500 °C and different GHSV were conducted (Fig. 3). The equilibrium conversion at the same conditions is also shown in Fig. 3.

At the GHSV of 30,000 h^{-1}, the conversion over three out of four catalysts approached the equilibrium conversion. It should be noted, however, that even though the GHSV of 30,000 h^{-1} is the lowest applied in this study, it is higher than that reported in similar work in literature [15,23,50–52], considering also that no diluent gas (He or N_2) is fed into the reactor during the reforming tests. The fact that most of the proposed catalysts approach equilibrium conversion under these conditions, indicate their high activity in the low temperature range. Increase in the GHSV resulted in decrease in the conversion as was expected. At 70,000 h^{-1} product distribution is controlled by kinetics over all catalysts, thus enabling the comparative investigation. The composition of the dry outlet stream is shown in Table 3 in comparison to the equilibrium predicted values. Despite the non-favorable conditions for the steam reforming reaction (T = 500 °C) about 50–60% of the outlet dry gas consists of produced hydrogen. The concentration of CO is below 2% over all catalysts indicating that they are also very active in the WGS reaction. This makes the tested catalysts, highly advantageous in their application in membrane reformers where CO is a major poison [53,54]. It should be emphasized, also, that the composition reported in Table 3 is referred to experimental results in the absence of membrane. The presence of the membrane and, consequently, the in situ removal of produced hydrogen would lead to equilibrium shift of both the reforming and the WGS reaction toward the products, i.e., hydrogen and CO_2. As a result the consumption of CO in the WGS would be enhanced and its concentration in the exit gas would be even lower. Experimental and modeling results in similar membrane reforming systems report a CO molar fraction of less than 0.02 in the effluent stream (dry basis) [9,10].

The effect of the reaction temperature in methane steam reforming at GHSV 70,000 h^{-1} is depicted in Fig. 4. The catalysts show methane conversion in the range of 36–46% at 550 °C, which corresponds to 60–77% of the equilibrium predicted value. As the temperature decreases, conversion is lower and the differences among the catalysts are more pronounced. Higher CH_4 conversion among the ZrLa supported catalysts was observed for Rh(1)ZrLa, achieving 75–85% of the equilibrium predicted conversion at the temperature range of 400–550 °C, while Ni(10)ZrLa showed moderate activity and was significantly affected by the temperature decrease. Ni(10)CeZrLa showed better performance than Ni(10)ZrLa approaching the equilibrium conversion by 68% at 550 °C. The dispersion of Ni was found to be slightly lower for Ni(10)CeZrLa, thus higher conversion depicts the effect of the presence of CeO_2 in the support. Analogous results were reported by Roh et al. [44] about the performance of Ni/Ce–ZrO_2 and Ni/La–ZrO_2 in methane steam reforming at 750 °C, concluding that Ce is preferable modifier than La. The moderate performance of Ni(10)ZrLa could be the result of high activation energy, which is another parameter that affects the kinetics of the reaction over a catalyst. Kinetic investigation over the reported catalysts is currently in progress. Rh(1)CeZrLa showed high conversion, but not as much as Rh(1)ZrLa, thus, the above mentioned effect of CeO_2 is not observed in this case. On the other hand, the dispersion of Rh(1)ZrLa is higher than Rh(1)CeZrLa which clearly affects their performance.

The effect of the partial pressure of methane (by varying the H_2O/CH_4 molar ratio) at constant GHSV on the performance of the catalysts was also investigated and the results are shown in Fig. 5. Almost equilibrium conversion was obtained over Rh(1)ZrLa catalyst at P_{CH4} of 0.33 and 0.5. Ni(10)CeZrLa and Rh(1)CeZrLa showed also good performance at P_{CH4} of 0.33 and the obtained conversion was 26% and 23.5% respectively. The lowest conversion among the catalysts under investigation was observed for Ni(10)ZrLa. In fact, the obtained conversion was hardly affected by the increase in the P_{CH4} at 500 °C over this catalyst. However, it should be noted that the obtained conversion at different P_{CH4} and constant GHSV is the result of two opposite effects. Conversion is positively affected by the increase in methane partial pressure [13]. On the other hand, under constant GHSV, increase in the partial pressure results in decrease in the contact time of methane (W/F_{CH4}), which has a negative effect on the conversion. In order to show the net effect of P_{CH4}, results are also expressed in terms of methane consump-

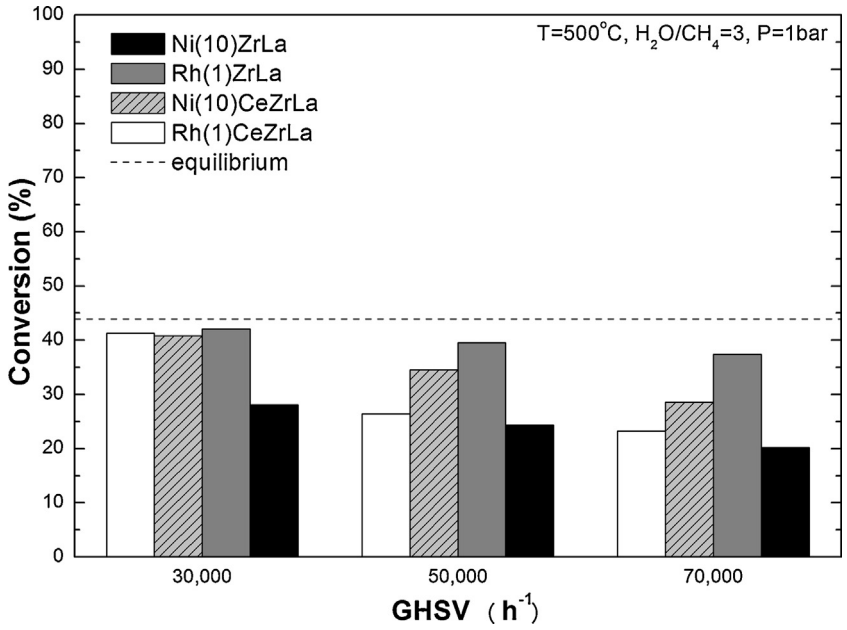

Fig. 3. Effect of GHSV on the CH_4 conversion over methane steam reforming. Conditions: $T = 500\,^{\circ}C$, $P = 1$ bar, $H_2O/CH_4 = 3$.

Table 3
Outlet gas composition (dry basis) in steam reforming of methane ($T = 500\,^{\circ}C$, GHSV = 70,000 h^{-1}, $H_2O/CH_4 = 3$).

	H_2 (%)	CH_4 (%)	CO (%)	CO_2 (%)
Ni(10)ZrLa	47.68	41.23	0.77	10.32
Rh(1)ZrLa	61.15	24.33	1.51	13.01
Ni(10)CeZrLa	53.40	32.88	1.67	11.48
Rh(1)CeZrLa	50.64	37.91	0.67	10.78
Equilibrium	62.94	20.79	2.14	14.13

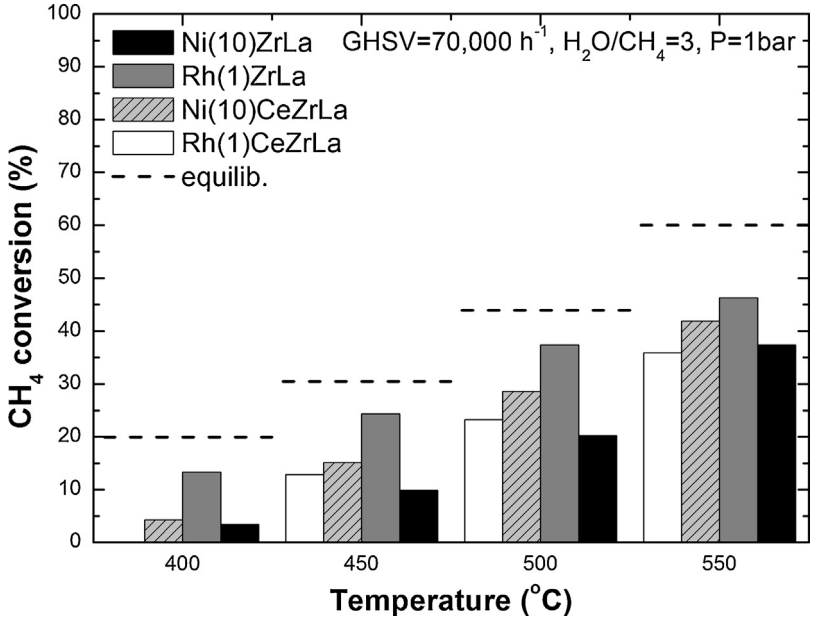

Fig. 4. Effect of temperature on methane conversion in methane steam reforming over M(x)ZrLa and M(x)CeZrLa catalysts. Conditions: $P = 1$ bar, GHSV = 70,000 h^{-1}, $H_2O/CH_4 = 3$.

tion rate per metal surface area (Fig. 5). The surface rate of CH_4 is increased by the increase in P_{CH4} over all catalysts, with the exception of Rh(1)ZrLa. The rate over the latter catalyst seems not to be affected by the increase in P_{CH4} from 0.33 to 0.5 maybe due to approaching equilibrium conditions.

3.3. Biogas steam reforming

In order to simulate biogas, a mixture of CH_4 and CO_2 with a molar ratio of 1 was used. The reaction of methane with carbon dioxide (dry reforming reaction) is more endothermic than the

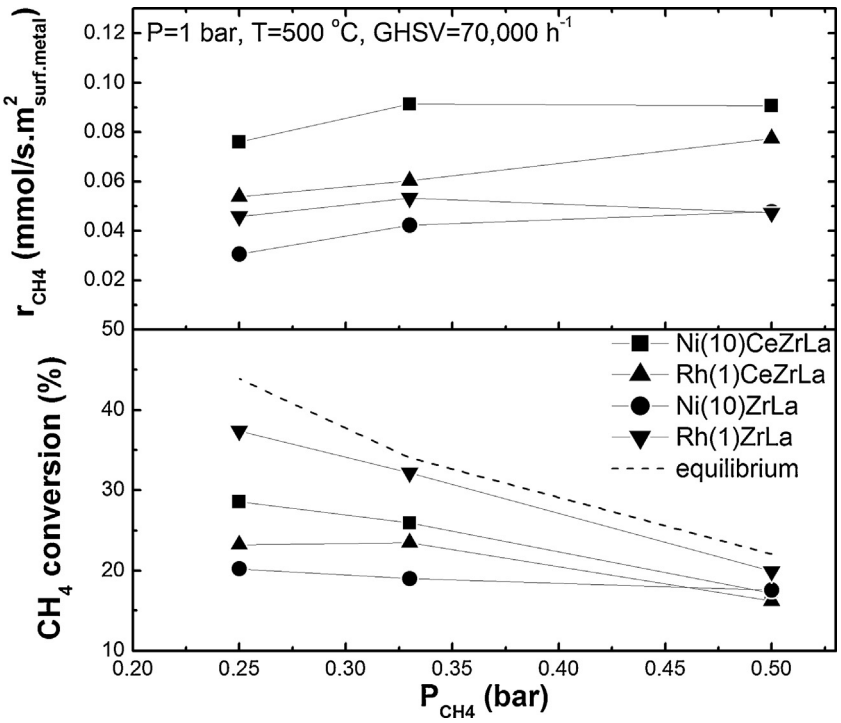

Fig. 5. Effect of partial pressure of methane in the feed stream (H_2O/CH_4 ratio) in methane steam reforming. Conditions: $P = 1$ bar, GHSV = 70,000 h^{-1}, $T = 500\,^{\circ}C$.

reaction of methane with steam (steam reforming). So, due to the high partial pressure of steam in the feed and the low temperature of operation, CO_2 contained in model biogas is probably not involved in methane reforming [55–57].

The performance of the catalysts in model biogas steam reforming at low temperature was investigated at atmospheric pressure, GHSV of 30,000 h^{-1} and H_2O/CH_4 of 3. The conversion of methane as a function of temperature is shown in Fig. 6 and is compared to that of equilibrium conditions.

Increase in the reaction temperature results in higher methane conversion over all catalysts. Ni(10)CeZrLa exhibited the optimum performance, approaching the equilibrium conversion by 87–90% in the temperature range of 450–550 °C, while conversion over Rh(1)ZrLa reached the equilibrium value by 75–82% at the same temperature range. It should be noted also, that the presence of CO_2 resulted in higher CO content in the effluent dry gas (results not shown) than in the methane steam reforming tests, due to the effect of the reverse WGS reaction. However, it was less than 5% over all catalysts for the temperature range of 400–500 °C. The effect of the reverse WGS was stronger at the temperature of 550 °C, reaching the content of almost 6–8%.

It is apparent that the presence of CO_2 in the gas feed the obtained conversion is lower compared to pure CH_4 feed. The difference on the obtained conversion between steam reforming of methane and biogas is attributed to both the lower partial pressure of CH_4 and steam in the reaction mixture as well as to the possible inhibitory effect of CO_2 to the overall reaction kinetics. The effect of CO_2 on the overall reaction kinetics is different for each catalyst, thus modification of the ranking of the catalysts with respect to that of methane steam reforming was observed. The expression of the catalytic results in terms of methane conversion depicts the overall performance of the catalyst and is very important for future industrial applications such as the proposed process. However, in order to better understand the activity in low temperature steam reforming, results may also be expressed in terms of the rate of CH_4 consumption per metal surface area (Fig. 7). On this basis, Ni(10)CeZrLa showed the highest intrinsic activity in the reforming of methane and model biogas followed by Rh(1)CeZrLa. On the other hand, Ni(10)ZrLa showed the least promising activity, even though both surface area and metal dispersion were higher than Ni(10)CeZrLa. It should be stressed also that the reaction rate over a catalyst is not only a matter of active site density but also a matter of interaction of the reactants with the catalytic surface, depicted by the activation energy. The low CH_4 consumption rate over Ni(10)ZrLa could be the result of high activation energy of the reaction.

The comparative analysis of the catalytic performance in steam reforming of both methane and biogas, gave information about the effect of the support on the activity. When La_2O_3–ZrO_2 was used as support, the Rh-based catalyst showed clearly better performance than the Ni-based catalyst. On the other hand, among the La_2O_3–CeO_2–ZrO_2 supported catalysts the inverse phenomenon is observed. Wei and Iglesia [4] reported that the effect of support lies in the dispersion of the active metal and does not affect the intrinsic activity. However, is has been widely discussed in the literature [14,22,58,59] that ceria containing supports play an active role in the reforming mechanism through the activation of steam and strongly enhance the reforming rate by oxygen back spillover process. ZrO_2 has also been found to participate in the steam reforming mechanism at 500 °C due to formation of surface hydroxyl groups [15]. In this work, it is believed that the effect of ZrLa support in the reforming rate is moderate, if any, and that it is the positive effect of CeZrLa support that might contribute to the higher activity of Ni(10)CeZrLa catalyst than the Rh counterpart. Additionally, it should be noted that Rh-based catalysts are prepared from chloride precursors. It is known that Cl^- ions are difficult to remove by calcination and reduction treatment, so their presence on Rh-based catalysts cannot be excluded. In this case, Cl^- ions may hinder the oxygen transfer from the ceria-containing support to the metal [36,60,61]. This might also be a reason of lower intrinsic activity observed for Rh(1)CeZrLa than that of Ni(10)CeZrLa in both methane and biogas steam reforming. The higher intrinsic activity of Ni among the CeZrLa-supported catalysts, in opposition to that reported in literature [4,62] might also be due to the lower

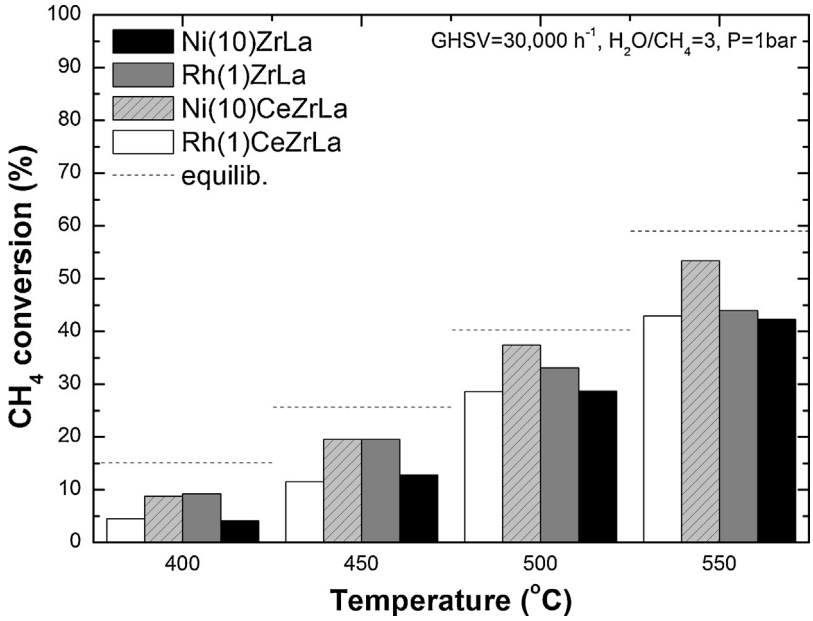

Fig. 6. Effect of temperature on methane conversion during biogas steam reforming. Conditions: $CH_4/CO_2 = 1$, $P = 1$ bar, GHSV = 30,000 h^{-1}, $H_2O/CH_4 = 3$.

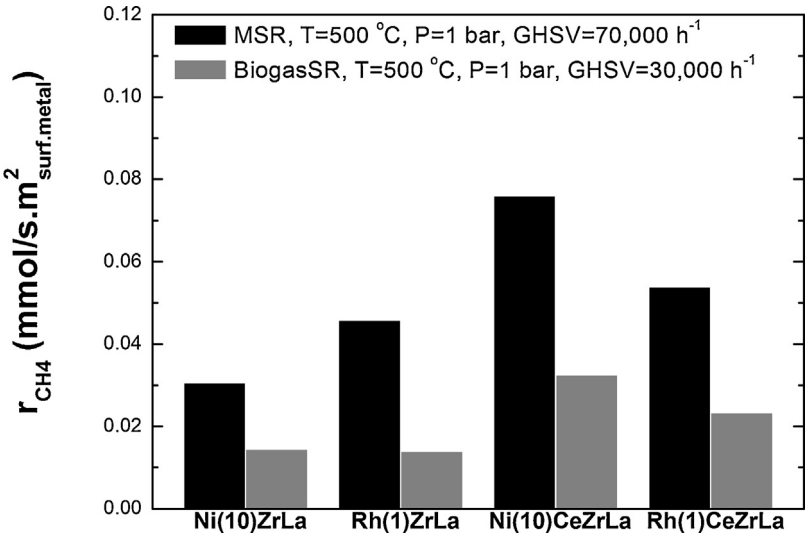

Fig. 7. Catalytic activity assessment in methane and model biogas steam reforming. Conditions: (a) MSR: $P = 1$ bar, GHSV = 70,000 h^{-1}, $T = 500\,^{\circ}C$, $H_2O/CH_4 = 3$. (b) Model biogas SR: $CH_4/CO_2 = 1$, $P = 1$ bar, GHSV = 30,000 h^{-1}, $T = 500\,^{\circ}C$, $H_2O/CH_4 = 3$.

temperature range used in this work. The effect of the temperature on the reaction rate is expressed by the Arrhenius equation with the parameters being the pre-exponential factor and the activation energy. Differences in the activation energy of the reaction over Ni(10)CeZrLa and Rh(1)CeZrLa, result in different influence of the performance by the temperature, which in turn may lead to inverse ranking when the catalysts are tested at different temperature.

3.3.1. *Preliminary stability evaluation*

Preliminary investigation on the stability of the catalysts was conducted at atmospheric pressure, temperature of 500 °C and H_2O/CH_4 of 3. Model biogas was selected as feed type for this evaluation because the high content of CO_2 may contribute to the accumulation of carbonaceous deposits [40,41]. Additionally, due to the low temperature applied, the presence of CO_2 may also affect the oxidation state of active metal leading to deactivation. The stability of Ni-based catalysts was evaluated based on 35-h-tests. Since Rh-based catalysts are well known to be more resistant to deactivation (e.g., by coke formation) [5], the duration of the stability tests over these catalysts was extended to 55 h. The results of the preliminary stability tests in terms of methane conversion with time on stream are depicted in Fig. 8.

Ni(10)ZrLa showed less stable behavior among the Ni-based catalysts, where the initial conversion was decreased by ca. 30% after 35 h on stream. A deactivation of ca. 15% after 55 h on stream was observed for Rh(1)ZrLa, which was proved less stable than Rh(1)CeZrLa. On the other hand, Ni(10)CeZrLa and Rh(1)CeZrLa showed fairly constant conversion and the deactivation was <5% after 35 h and 55 h on stream respectively. The higher stability observed by the catalysts supported on La_2O_3–CeO_2–ZrO_2 compared to those supported on La_2O_3–ZrO_2, highlights the importance of the presence of ceria in the support oxide in the resistance to deactivation factors such as carbon formation.

Based on their higher stability as well as intrinsic activity, Ni(10)CeZrLa and Rh(1)CeZrLa were selected for further investigation under high pressure reforming conditions.

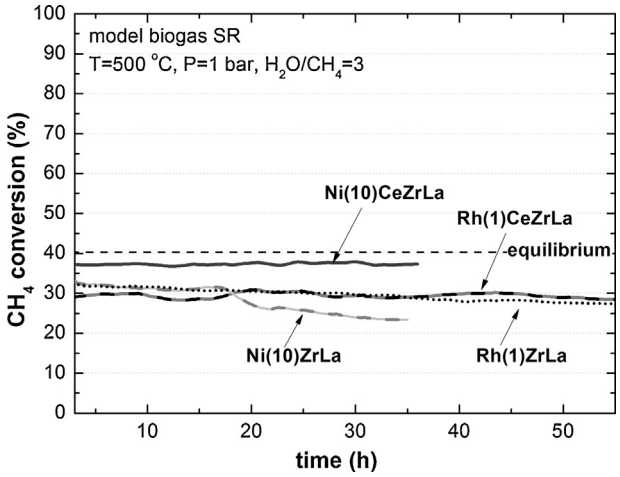

Fig. 8. Methane conversion obtained during preliminary stability testing. Conditions: model biogas feed ($CH_4/CO_2 = 1$), $H_2O/CH_4 = 3$, $T = 500\,^{\circ}C$, $P = 1$ bar, GHSV = 30,000 h^{-1}.

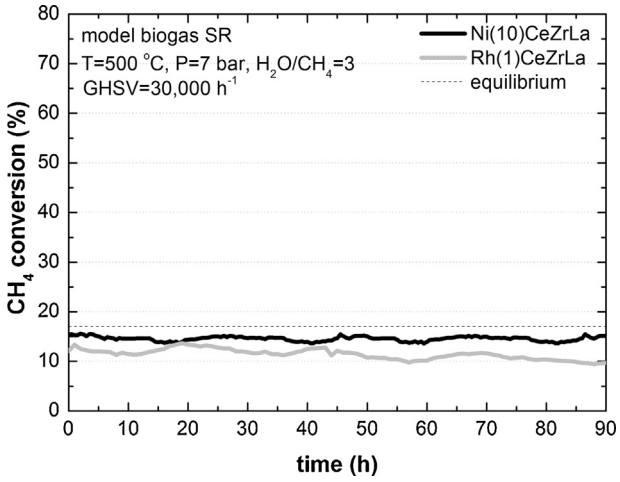

Fig. 9. Methane conversion during stability under severe conditions over Rh(1)/CeZrLa and Ni(10)CeZrLa catalyst. Conditions: model biogas feed, ($CH_4/CO_2 = 1$), $H_2O/CH_4 = 3$, $T = 500\,^{\circ}C$, $P = 7$ bar, GHSV = 30,000 h^{-1}.

3.3.2. Stability of Ni(10)CeZrLa and Rh(1)CeZrLa at high pressure

Further investigation on the stability of the selected catalysts Ni(10)CeZrLa and Rh(1)CeZrLa was realized under high pressure (7 bar) in order to simulate the conditions of the proposed membrane reformer [6]. The duration of the stability tests was 90 h using model biogas as feed ($H_2O/CH_4/CO_2 = 3/1/1$).

Very stable behavior even after 90 h on stream (Fig. 9) was observed for Ni(10)CeZrLa. The stability can be ascribed to the presence of ceria in the support which provides active oxygen for the minimization of coke formation and also to the lanthana dopant, known for its thermal stabilization effect, and to the low affinity for coking [63–66]. The high mobility of oxygen formed by the decomposition of H_2O on the support surface and its diffusion through ceria facilitates the oxidation of any carbonaceous deposits formed [43]. In addition to effect of ceria, the presence of La_2O_3 contributes to the resistance in coke accumulation, though the reaction of active $La_2O_2CO_3$ with the deposited carbon species [26,67]. The conversion of methane over Rh(1)CeZrLa catalyst was decreased by ca. 16.7%. Since Rh-based catalysts are generally more resistant to coke formation than Ni-based catalysts, possible cause of deactivation might be sintering of the metal particles and/or change in the oxidation state due to the high partial pressure of CO_2 in the reaction mixture.

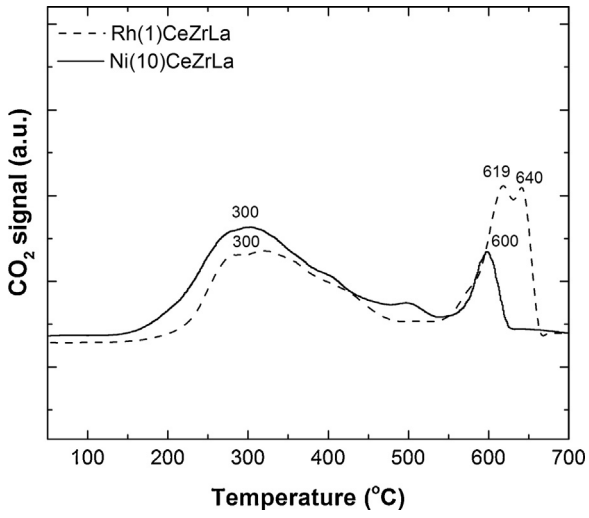

Fig. 10. TPO profiles of the catalysts used at model biogas steam reforming under high pressure for 90 h.

3.4. Characterization of used catalysts

The deposition of carbonaceous species on the catalytic surface during steam reforming of model biogas at high pressure was investigated by employing temperature programmed oxidation and hydrogenation techniques (TPO/TPH). The used samples were exposed to an oxidizing/reducing gas mixture, with increasing temperature and the formation of CO_2/CH_4 was continuously monitored in order to provide information about the nature and the quantity of carbon species.

The TPO profiles of the used catalysts are shown in Fig. 10. The CO_2 signal over the used Ni(10)CeZrLa is consisted of two main peaks. The wide peak at the temperature range of 200–550 °C, which corresponds to ca. 80% of the total CO_2 produced, can be ascribed to reactive carbon species [68]. The second peak, centered at 600 °C, is characteristic of the oxidation of filamentous carbon [69,70]. Peaks in the same temperature range are apparent in the TPO profile of the used Rh(1)CeZrLa corresponding to carbon species of similar reactivity. Amorphous carbon species that can be removed by oxidation below 550 °C, based on the relative peak area, correspond to about 60% of the total carbon formed on the surface of Rh(1)CeZrLa, while filamentous carbon seems to be slightly more difficult to oxide than in the case of Ni(10)CeZrLa.

The TPH profiles of the used Ni(10)CeZrLa and Rh(1)CeZrLa are presented in Fig. 11. Two main peaks are observed for Ni(10)CeZrLa catalyst with temperature of maximum hydrogenation at 254 °C and 560 °C. The low temperature peak can be ascribed to the hydrogenation of reactive carbon that is formed at the early stages of the reaction and is not responsible for deactivation, while the high temperature peak is referred to the hydrogenation of carbon filaments [71]. The CH_4 trace in the case of Rh(1)CeZrLa reveals two peaks in close proximity in the temperature range of 200–500 °C and a third peak at 568 °C. It should be noted that, according to the TPH profiles of both Ni(10)CeZrLa and Rh(1)CeZrLa, at least 80% of the total carbon accumulated can be effectively removed by the temperature of 500 °C. This is rather advantageous for industrial application; the catalyst can be regenerated by introducing part of the product stream without temperature increase and keep the catalyst in reduced state at the same time.

Quantification of carbonaceous deposits based on the TPO and TPH profiles are in very good agreement (Table 4). The amount of carbon determined on the Ni catalyst was ca. 0.05 wt% and is in line with the high stability observed under higher pressure. Quantification results are also expressed as the overall conversion of

Table 4
Quantification of deposited carbon determined by TPO and TPH.

Catalyst	TOS (h)	C wt% on catalyst		Conversion of inlet C ($CH_4 + CO_2$) to solid C (10^{-3}%)	
		TPO	TPH	TPO	TPH
Ni(10)CeZrLa	5	0.08	0.08	0.236	0.236
Ni(10)CeZrLa	50	0.12	0.08	0.035	0.024
Ni(10)CeZrLa	90	0.05	0.06	0.008	0.010
Rh(1)CeZrLa	90	0.14	0.19	0.023	0.031

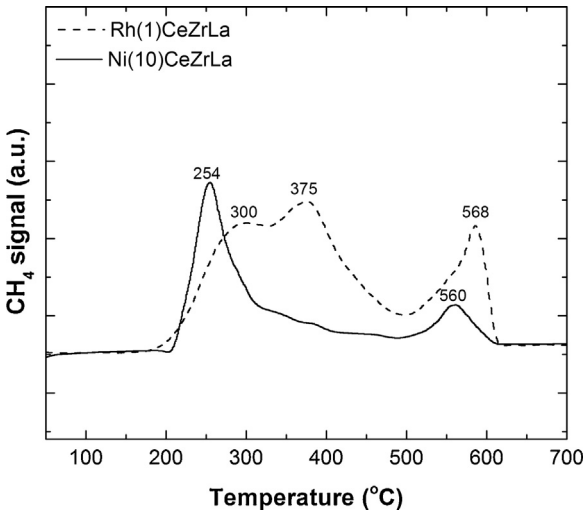

Fig. 11. TPH profiles of the catalysts used at model biogas steam reforming under high pressure for 90 h.

inlet carbon ($CH_4 + CO_2$) to solid carbon on the catalytic surface. The carbon content in the used Rh(1)CeZrLa is slightly higher, (ca. 0.15 wt%), corresponding to ca. 0.027×10^{-3}% conversion of carbon fed to the reactor to solid carbon. This might also be an effect of remaining Cl^- ions on the catalyst from the chlorinated precursor. The presence of Cl^- ions affects the acid-base properties of the catalyst [72–74]. The incorporation of basic metal oxides in the support such as La_2O_3, are expected to prevent carbon formation [75]. Consequently, compensation of the basic properties of the support due to the presence of Cl^- ions, could explain the slightly higher amount of carbon accumulated compared to Ni(10)CeZrLa (Table 4). However, the amount of carbon formed on Rh(1)CeZrLa was still in very low level and is highly unlikely to cause the observed deactivation. Loss of initial activity might be due to particle agglomeration or change in the oxidation state of metal nanoparticles.

The progress of carbon formation on Ni(10)CeZrLa with time on stream was also investigated. TPO and TPH analysis was performed on the catalyst after 5, 50, and 90 h of steam reforming of model biogas at 500 °C and 7 bar (Fig. 12 a and b). It is clear that the nature of the carbon species is not significantly affected by the reaction time since the TPO and TPH profiles after 5 and 50 h are very similar to that after 90 h of reaction. The relative intensity of the high temperature peak with respect to the low temperature peak indicates that slow polymerization of reactive carbon may occur. In addition, the quantification results show that the total amount of carbon is not increasing with time on stream probably due to equilibration of carbon accumulation and gasification processes (Table 4). Carbon seems to be formed at the early stages of the reaction and no build-up of the carbonaceous deposits occurs with time on stream. Based on the carbon content on the used catalysts and the duration of the test, the average conversion of inlet C to solid C in each test can be estimated. Since the amount of total carbon depositions are

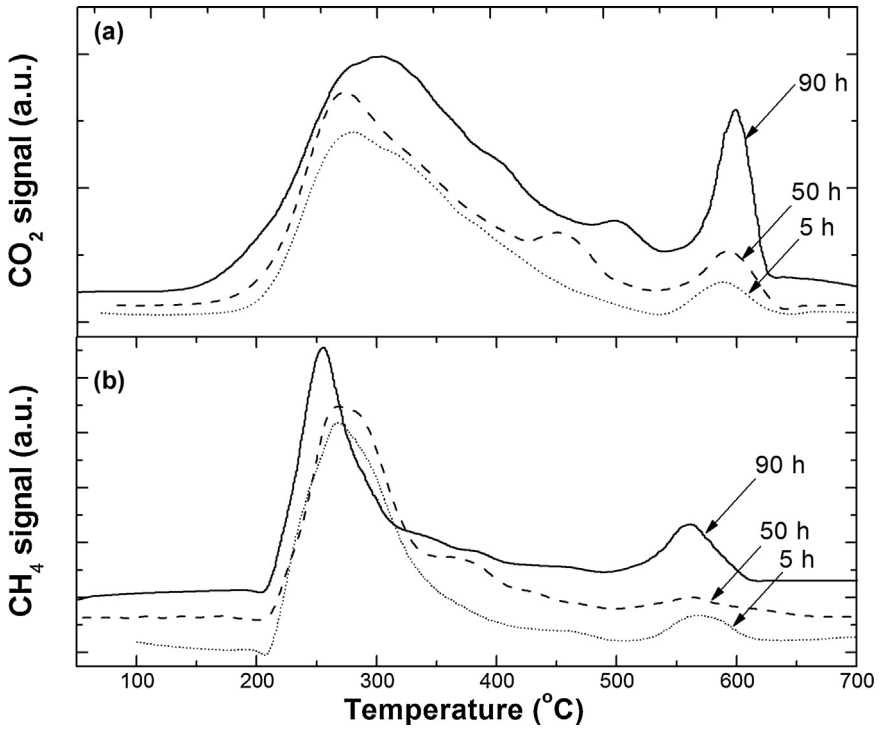

Fig. 12. TPO (a) and TPH (b) of Ni(10)CeZrLa exposed to steam reforming of model biogas at high pressure for different reaction time.

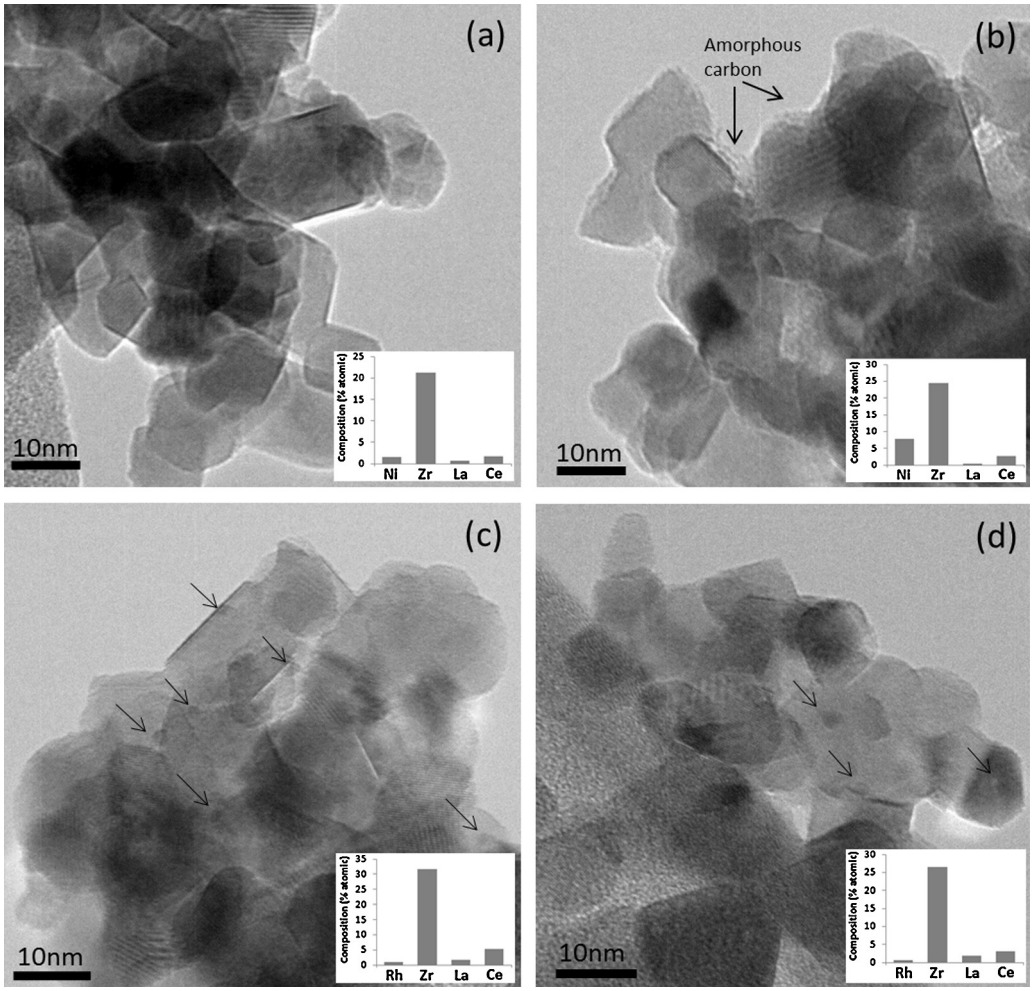

Fig. 13. TEM images of (a) Ni(10)CeZrLa after reduction treatment, (b) Ni(10)CeZrLa after stability test at high pressure, (c) Rh(1)CeZrLa after reduction, (d) Rh(1)CeZrLa after stability test at high pressure.

in the same level and the duration of the test is different, the net conversion of gaseous inlet C to solid C decreases by an order of magnitude.

The TEM technique was employed for the investigation of the morphology of the best performing catalysts after the stability test at high pressure. Some representative images are reported in Fig. 13.

Ni(10)CeZrLa after reduction treatment (Fig. 13a) is characterized by high crystallinity. Due to low contrast between Ni and the crystalline support, it was not possible to distinguish the Ni particles and extract safe information about the metal crystallite size. EDS spectra of uniform-like areas, such as that shown in Fig 13a confirmed the existence of Ni, which is probably in a similar particle size range as the support. It should be noted also that several large Ni particles (ca. 50 nm) were detected (not shown), which might be responsible for the broad reduction peak of NiO in the TPR (Fig. 2), but these agglomerates were not considered to be representative. The TEM image of the Ni(10)CeZrLa after 90 h in steam reforming of model biogas at high pressure is shown in Fig 12b. No apparent agglomeration is observed compared to the reduced sample. Amorphous carbon was detected around the particles probably in contact with Ni, since EDS analysis showed relatively high atomic concentration of Ni in these areas. The presence of amorphous carbon was also indicated by the low oxidation peak in TPO and TPH experiments as discussed earlier. On the other hand, the presence of carbon filaments, indicated by TPO and TPH was not confirmed by TEM, probably due to the very low quantity.

Fig. 13c presents the morphology of Rh(1)CeZrLa after reduction treatment. Size and morphology of the support is similar to that of Ni(10)CeZrLa. Crystallites in the size range of 10–30 nm corresponding to the support are apparent. Some smaller particles could also be observed which are probably Rh particles (3–6 nm). The catalyst after reaction at high pressure for 90 h retained its initial morphology and no metal agglomeration was observed that could cause loss of activity. The only type of carbon traced was that of onion-like amorphous type which however was not in contact with the particles but was located occasionally between aggregates. This finding further supports the possibility of remaining Cl^- ions affecting the carbon resistance of the support. As a result, carbon formation cannot be considered responsible for the small deactivation observed during the stability test. Changes in the oxidation state of the metal nanoparticles due to the low temperature of operation and/or the high partial pressure of CO_2 in the feed, might have affected its performance.

4. Conclusions

In this work, the catalytic performance of four catalysts (Ni/La_2O_3–CeO_2–ZrO_2, Rh/ La_2O_3–CeO_2–ZrO_2, Ni/La_2O_3–ZrO_2, and Rh/La_2O_3–ZrO_2) was investigated in steam reforming of methane and model biogas at the temperature range of 400–550 °C. A comparative analysis of the catalysts is reported based on their performance in different operating conditions (temperature, GHSV, H_2O/CH_4 molar ratio and feed type). Higher activity was observed

for Ni(10)CeZrLa and Rh(1)CeZrLa, probably due to the active role of reduced ceria contributing to the dissociation of steam and the oxygen spillover effect.

Preliminary stability evaluation in model biogas steam reforming at ambient pressure highlighted the importance of CeO_2 in the support, since Ni(10)CeZrLa and Rh(1)CeZrLa were the most stable catalysts and were selected for further investigation at high pressure in 90-h-stability tests.

Ni(10)CeZrLa showed remarkably stable behavior after 90 h of model biogas steam reforming at high pressure and minimum amount of carbon formation (0.05 wt%). Rh(1)CeZrLa showed a mild deactivation of 16.7% after 90 h, which, however, cannot be attributed to metal sintering (TEM analysis) or to carbon accumulation but probably to change in the oxidation state of the metal. The low amount of carbon formed over both catalysts after 90 h and resistance in sintering effects are ascribed to the presence of ceria in the support which provides active oxygen for the minimization of coke formation and also to the lanthana dopant, known for its thermal stabilization effect and low affinity for coking.

TPO and TPH analysis of the carbonaceous deposits showed that the dominating type of carbon is highly reactive and can be easily removed by oxidation or hydrogenation at 500-550 °C. This fact makes Ni(10)CeZrLa even more promising for the proposed low temperature process, since the catalyst can be hydrogenated (remove carbon and maintain the active metal in reduced state) by using part of the H_2 production stream without further heating of the reactor. Analysis of the carbonaceous deposits after different reaction time showed that the total amount of carbon over Ni(10)CeZrLa is not increased with time on stream, as a result of equilibration between accumulation and gasification effects.

Acknowledgements

The research leading to the results reported in this paper has received funding from the European Union's Seventh Framework Programm (FP7/2007-2013) for the Fuel Cells and Hydrogen Joint Technology Initiative, for CoMETHy project under grant agreement n° 279075. The contribution of Prof. Maria-Christina Annesini and Dr. Alberto Giaconia is greatly acknowledged. Mel Chemicals is acknowledged for providing the catalytic supports used in this work. Dr. Andreas Delimitis from the Analytical Service Unit of CPERI/CERTH is also acknowledged for the characterization of catalysts by TEM analysis.

References

[1] K. Aasberg-Petersen, I. Dybkjær, C.V. Ovesen, N.C. Schjødt, J. Sehested, S.G. Thomsen, J. Nat. Gas Sci. Eng. 3 (2011) 423–459.
[2] J.R. Rostrup-Nielsen, J. Sehested, J.K. Nørskov, Adv. Catal. 47 (2002) 65–139.
[3] J.R. Rostrup-Nielsen, Catal. Today 111 (2006) 4–11.
[4] J. Wei, E. Iglesia, J. Catal. 224 (2004) 370–383.
[5] D.L. Trimm, Catal. Today 49 (1999) 3–10.
[6] A. Giaconia, L. Turchetti, G. Monteleone, B. Morico, G. Iaquaniello, K. Shabtai, M. Sheintuch, D. Boettge, J. Adler, V. Palma, S. Voutetakis, A. Lemonidou, M.C. Annesini, M. Den Exter, H. Balzer, Chem. Eng. Trans. 35 (2013) 433–438.
[7] S. Lægsgaard Jørgensen, P.E.H. Nielsen, P. Lehrmann, Catal. Today 25 (1995) 303–307.
[8] J. Tong, Y. Matsumura, Catal. Today 111 (2006) 147–152.
[9] A. Kyriakides, L. Rodríguez-García, S. Voutetakis, D. Ipsakis, P. Seferlis, S. Papadopoulou, Int. J. Hydrogen Energy 39 (2014) 4749–4760.
[10] M. Patrascu, M. Sheintuch, Chem. Eng. J. 262 (2015) 862–874.
[11] A. Giaconia, M. de Falco, G. Caputo, R. Grena, P. Tarquini, L. Marrelli, AIChE J. 54 (2008) 1932–1944.
[12] P. Ferreira-Aparicio, M.J. Benito, J.L. Sanz, Catal. Rev. Sci. Eng. 47 (2005) 491–588.
[13] S. Lee, Methane and its Derivatives, M. Dekker, New York, 1997.
[14] K. Polychronopoulou, C.M. Kalamaras, A.M. Efstathiou, Rec. Patent Mater. Sci. 4 (2011) 122–145.
[15] Y. Matsumura, T. Nakamori, Appl. Catal. A: Gen. 258 (2004) 107–114.
[16] S.D. Angeli, G. Monteleone, A. Giaconia, A.A. Lemonidou, Int. J. Hydrogen Energy 39 (2014) 1979–1997.
[17] G. Nahar, V. Dupont, Renew. Sustain. Energy Rev. 32 (2014) 777–796.
[18] S. Gopalakrishnan, M.G. Faga, I. Miletto, S. Coluccia, G. Caputo, S. Sau, A. Giaconia, G. Berlier, Appl. Catal. B: Environ. 138–139 (2013) 353–361.
[19] H.S. Roh, I.H. Eum, D.W. Jeong, Renew. Energy 42 (2012) 212–216.
[20] D.A.J.M. Ligthart, R.A. Van Santen, E.J.M. Hensen, J. Catal. 280 (2011) 206–220.
[21] M. Sekine, M. Matsukata, E. Kikuchi, Catal. Today 171 (2011) 116–125.
[22] M.H. Halabi, M.H.J.M. De Croon, J. Van Der Schaaf, P.D. Cobden, J.C. Schouten, Appl. Catal. A Gen. 389 (2010) 68–79.
[23] K. Kusakabe, K. Sotowa, T. Eda, Y. Iwamoto, Fuel Process. Technol. 86 (2004) 319–326.
[24] J.S. Moura, J.D.S.L. Fonseca, N. Bion, F. Epron, T.D.F. Silva, C.G. Maciel, J.M. Assaf, M.D.C. Rangel, Catal. Today 228 (2014) 40–50.
[25] A.A. Lemonidou, E.C. Vagia, J.A. Lercher, ACS Catal. 3 (2013) 1919–1928.
[26] D.A.J.M. Ligthart, J.A.Z. Pieterse, E.J.M. Hensen, Appl. Catal. A Gen. 405 (2011) 108–119.
[27] L. Kundakovic, M. Flytzani-Stephanopoulos, Appl. Catal. A Gen. 171 (1998) 13–29.
[28] U. Izquierdo, V.L. Barrio, K. Bizkarra, A.M. Gutierrez, J.R. Arraibi, L. Gartzia, J. Bañuelos, I. Lopez-Arbeloa, J.F. Cambra, Chem. Eng. J. 238 (2014) 178–188.
[29] A.F. Lucrédio, J.M. Assaf, E.M. Assaf, Fuel Process. Technol. 102 (2012) 124–131.
[30] K. Lin, H. Chang, A.C.C. Chang, Int. J. Hydrogen Energy 37 (2012) 15696–15703.
[31] D.G. Avraam, T.I. Halkides, D.K. Liguras, O.A. Bereketidou, M.A. Goula, Int. J. Hydrogen Energy 35 (2010) 9818–9827.
[32] T. Sato, T. Suzuki, M. Aketa, Y. Ishiyama, K. Mimura, N. Itoh, Chem. Eng. Sci. 65 (2010) 451–457.
[33] V. Perrichon, L. Retailleau, P. Bazin, M. Daturi, J.C. Lavalley, Appl. Catal. A Gen. 260 (2004) 1–8.
[34] S. Bernal, J.J. Calvino, G.A. Cifredo, A. Laachir, V. Perrichon, J.M. Herrmann, Langmuir 10 (1994) 717–722.
[35] S. Bernal, F.J. Botana, J.J. Calvino, M.A. Cauqui, G.A. Cifredo, A. Jobacho, J.M. Pintado, J.M. Rodríguez-Izquierdo, J. Phys. Chem. 97 (1993) 4118–4123.
[36] D.I. Kondarides, X.E. Verykios, J. Catal. 174 (1998) 52–64.
[37] T. De Freitas Silva, J.A.C. Dias, C.G. MacIel, J.M. Assaf, Catal. Sci. Technol. 3 (2013) 635–643.
[38] R. Geyer, J. Hunold, M. Keck, P. Kraak, A. Pachulski, R. Schödel, Chem. Ing. Tech. 84 (2012) 160–164.
[39] G. Bergeret, P. Gallezot, Handbook of Heterogeneous Catalysis, in: G. Ertl, H. Knözinger, J. Weitkamp (Eds.), VCH, Weinheim, 1997, p. 427.
[40] J. Zhao, W. Zhou, J. Ma, Int. J. Hydrogen Energy 39 (2014) 13429–13436.
[41] W.D. Zhang, B.S. Liu, C. Zhu, Y.L. Tian, Appl. Catal. A Gen. 292 (2005) 138–143.
[42] J.A. Wang, T. Lopez, X. Bokhimi, O. Novaro, J. Mol. Catal. A: Chem. 239 (2005) 249–256.
[43] E.C. Vagia, A.A. Lemonidou, J. Catal. 269 (2010) 388–396.
[44] H.S. Roh, K.W. Jun, S.E. Park, J. Ind. Eng. Chem. 9 (2003) 261–266.
[45] M.H. Youn, J.G. Seo, I.K. Song, Int. J. Hydrogen Energy 35 (2010) 3490–3498.
[46] L. Cao, C. Ni, Z. Yuan, S. Wang, Catal. Lett. 131 (2009) 474–479.
[47] S.K. Ram, M.N. Islam, S. Kumar, P. Roca, I. Cabarrocas, Mater. Sci. Eng. B 159–160 (2009) 34–37.
[48] Y. Li, X. Wang, C. Xie, C. Song, Appl. Catal. A: Gen. 357 (2009) 213–222.
[49] H. Roh, K. Jun, W. Dong, J. Chang, S. Park, Y. Joe, J. Mol. Catal. A: Chem. 181 (2002) 137–142.
[50] H.S. Roh, K.W. Jun, Bull. Kor. Chem. Soc. 30 (2009) 153–156.
[51] L.Q. Nguyen, L.C. Abella, S.M. Gallardo, H. Hinode, React. Kinet. Catal. Lett. 93 (2008) 227–232.
[52] Z.W. Liu, K.W. Jun, H.S. Roh, S.E. Park, J. Power Sources 111 (2002) 283–287.
[53] A. Basile, A. Iulianelli, T. Longo, S. Liguori, M. De Falco, Membrane Reactors for Hydrogen production Processes, in: M. De Falco, L. Marrelli, G. Iaquaniello (Eds.), Springer, London, 2011, pp. 21–55.
[54] E. Kikuchi, Catal. Today 56 (2000) 97–101.
[55] M.A. Soria, C. Mateos-Pedrero, A. Guerrero-Ruiz, I. Rodríguez-Ramos, Int. J. Hydrogen Energy 36 (2011) 15212–15220.
[56] S.C. Baek, J.W. Bae, J.Y. Cheon, K.W. Jun, K.Y. Lee, Catal. Lett. 141 (2011) 224–234.
[57] Ş. Özkara-Aydınoğlu, Int. J. Hydrogen Energy 35 (2010) 12821–12828.
[58] A. Lamacz, A. Krzton, Int. J. Hydrogen Energy 38 (2013) 8772–8782.
[59] W.S. Dong, H.S. Roh, K.W. Jun, S.E. Park, Y.S. Oh, Appl. Catal. A Gen. 226 (2002) 63–72.
[60] E.O. Jardim, S. Rico-Francés, F. Coloma, J.A. Anderson, J. Silvestre-Albero, A. Sepúlveda-Escribano, J. Colloid Interface Sci. 443 (2015) 45–55.
[61] C. Descorme, D. Duprez, Appl. Catal. A Gen. 202 (2000) 231–241.
[62] J. Wei, E. Iglesia, J. Catal. 225 (2004) 116–127.
[63] S.Y. Foo, C.K. Cheng, T. Nguyen, E.M. Kennedy, B.Z. Dlugogorski, A.A. Adesina, Catal. Commun. 26 (2012) 183–188.
[64] J. Huang, R. Ma, T. Huang, A. Zhang, W. Huang, J. Nat. Gas Chem. 20 (2011) 465–470.
[65] J.F. Múnera, S. Irusta, L.M. Cornaglia, E.A. Lombardo, D. Vargas Cesar, M. Schmal, J. Catal. 245 (2007) 25–34.
[66] V.A. Tsipouriari, X.E. Verykios, J. Catal. 187 (1999) 85–94.
[67] V.A. Tsipouriari, X.E. Verykios, Catal. Today 64 (2001) 83–90.
[68] P.O. Graf, B.L. Mojet, J.G. van Ommen, L. Lefferts, Appl. Catal. A: Gen. 332 (2007) 310–317.
[69] N.V. Parizotto, K.O. Rocha, S. Damyanova, F.B. Passos, D. Zanchet, C.M.P. Marques, J.M.C. Bueno, Appl. Catal. A: Gen. 330 (2007) 12–22.

[70] K.M. Hardiman, C.G. Cooper, A.A. Adesina, R. Lange, Chem. Eng. Sci. 61 (2006) 2565–2573.
[71] A. Olafsen, C. Daniel, Y. Schuurman, L.B. Råberg, U. Olsbye, C. Mirodatos, Catal. Today 115 (2006) 179–185.
[72] E.S. Vasiliadou, E. Heracleous, I.A. Vasalos, A.A. Lemonidou, Appl. Catal. B: Environ. 92 (2009) 90–99.
[73] B. Lin, R. Wang, X. Yu, J. Lin, F. Xie, K. Wei, Catal. Lett. 124 (2008) 178.
[74] B. Bachiller-Baeza, A. Guerrero-Ruíz, I. Rodríguez-Ramos, J. Catal. 229 (2005) 439–445.
[75] J. Liu, J. Jiang, Y. Pan, ChemCatChem 3 (2011) 529–541.